PNAS PLUS

Auxin minimum triggers the developmental switch from cell division to cell differentiation in the *Arabidopsis* root

Riccardo Di Mambro[a,1,2], Micol De Ruvo[a,b,c,1], Elena Pacifici[a], Elena Salvi[a], Rosangela Sozzani[d], Philip N. Benfey[e,f], Wolfgang Busch[g], Ondrej Novak[h], Karin Ljung[h], Luisa Di Paola[b], Athanasius F. M. Marée[c], Paolo Costantino[a], Verônica A. Grieneisen[c,3], and Sabrina Sabatini[a,i,3]

[a]Dipartimento di Biologia e Biotecnologie, Laboratory of Functional Genomics and Proteomics of Model Systems, Università di Roma, Sapienza, 00185 Rome, Italy; [b]Unit of Chemical-Physics Fundamentals in Chemical Engineering, Department of Engineering, Università Campus Bio-Medico di Roma, 00128 Rome, Italy; [c]Computational and Systems Biology, John Innes Centre, Norwich Research Park, Norwich NR4 7UH, United Kingdom; [d]Department of Plant and Microbial Biology, North Carolina State University, Raleigh, NC 27695; [e]Department of Biology, Duke University, Durham, NC 27708; [f]Howard Hughes Medical Institute, Duke University, Durham, NC 27708; [g]Gregor Mendel Institute, Austrian Academy of Sciences, Vienna Biocenter, 1030 Vienna, Austria; [h]Umeå Plant Science Centre, Department of Forest Genetics and Plant Physiology, Swedish University of Agricultural Sciences, SE-901 83 Umeå, Sweden; and [i]Istituto Pasteur-Fondazione Cenci Bolognetti, 00100 Rome, Italy

Edited by Sarah Hake, University of California, Berkeley, CA, and approved June 26, 2017 (received for review April 11, 2017)

In multicellular organisms, a stringent control of the transition between cell division and differentiation is crucial for correct tissue and organ development. In the *Arabidopsis* root, the boundary between dividing and differentiating cells is positioned by the antagonistic interaction of the hormones auxin and cytokinin. Cytokinin affects polar auxin transport, but how this impacts the positional information required to establish this tissue boundary, is still unknown. By combining computational modeling with molecular genetics, we show that boundary formation is dependent on cytokinin's control on auxin polar transport and degradation. The regulation of both processes shapes the auxin profile in a well-defined auxin minimum. This auxin minimum positions the boundary between dividing and differentiating cells, acting as a trigger for this developmental transition, thus controlling meristem size.

plant hormones | cell differentiation | root meristem | computational modeling

Pattern formation in multicellular organisms is established by signal molecules that position boundaries between regions of different cell behavior (1–3). The maintenance of these boundaries is essential to ensure the structural and functional integrity of adult organs. In plants, auxin acts as a signaling molecule providing diverse developmental outputs by interacting with different molecules and regulatory circuits in a spatially distributed manner (4–6). We have shown that in the *Arabidopsis* root, auxin interacts with cytokinin to position the boundary between dividing and differentiating cells (4).

Root tissues originate from asymmetric cell divisions of stem cells bordering a small group of organizing cells, the quiescent center (QC), necessary for their self-renewal activity. Together they form the stem cell niche (SCN). Stem cells generate daughter cells that proliferate within their respective files throughout the meristematic zone (MZ) (7, 8). At the transition boundary (TB), divisions cease and cells start to elongate, initiating differentiation (DFZ 1). The zone encompassing the TB of the different cell files is called the transition zone (TZ). Cells further elongate (DFZ 2) and eventually complete their differentiation program (DFZ 3) (Fig. 1).

A coordinated activity of these zones and thus the maintenance of the TZ position are essential to stabilize meristem size and to ensure continuous root growth. We have shown that at the TZ, the cytokinin-responsive transcription factor ARABIDOPSIS RESPONSE REGULATOR 1 (ARR1) inhibits the expression of the PIN auxin transport facilitators. It does so by directly activating transcription of the *SHORT HYPOCOTYL 2* (*SHY2*) gene, a repressor of auxin signaling (4). Conversely, auxin mediates degradation of the SHY2 protein sustaining the activity of the *PIN* genes (4).

However, while pinpointing the control of cytokinin on auxin transport (4), this circuit does not explain how cytokinin shapes the auxin distribution to generate an instructive signal that stabilizes the TZ. To this end, we combined a molecular genetic approach with computational modeling. We previously developed a model in which the activity and localization of PINs gives rise to a reflux loop sufficient to generate a graded distribution of auxin within the root tip, with a stable auxin maximum at the QC (9), which was later confirmed experimentally (10). In that model, the TZ, assumed to be governed by a low threshold value within a slowly expanding gradient, moved shootwards over long

Significance

The maintenance of boundaries between neighboring groups of distinct cell types is vital during development of multicellular organisms, as groups of cells with distinct functions must be kept physically separated to guarantee correct control of organ and body growth and function. In the *Arabidopsis* root, the transition zone is a developmental boundary in the meristem that separates dividing from differentiating cells. Here, we infer that a well-defined and tightly controlled minimum of the hormone auxin acts as a signal to establish the position of the transition zone by controlling the developmental switch from cell division to cell differentiation. We provide the mechanistic and genetic basis of how another hormone, cytokinin, controls and positions this auxin minimum, thus regulating root size.

Author contributions: V.A.G. and S.S. conceived the research; R.D.M. and M.D.R. planned experiments; R.D.M. performed experiments; R.D.M., M.D.R., and A.F.M.M. planned simulations; M.D.R. and A.F.M.M. performed simulations; A.F.M.M. developed the code for simulations; M.D.R. and A.F.M.M. implemented the code for simulations; R.S., P.N.B., and W.B. performed ChIP-chip experiments; E.P. and E.S. cloned genes; O.N. and K.L. performed auxin measurement; L.D.P. discussed experiments; P.C. discussed experiments; R.D.M., M.D.R., A.F.M.M., V.A.G., and S.S. discussed and interpreted all results; and R.D.M., M.D.R., A.F.M.M., V.A.G., and S.S. wrote the paper.

The authors declare no conflict of interest.

This article is a PNAS Direct Submission.

Freely available online through the PNAS open access option.

Data deposition: The data reported in this paper have been deposited in the Gene Expression Omnibus (GEO) database, https://www.ncbi.nlm.nih.gov/geo (accession no. GSE70595). The code and the scripts that generated all simulation outputs (graphs and images) are available on Bitbucket (https://bitbucket.org/mareelab/transitionzone).

[1]R.D.M. and M.D.R. contributed equally to this work.

[2]Present address: Dipartimento di Biologia, Università di Pisa, 56126 Pisa, Italy.

[3]To whom correspondence may be addressed. Email: veronica.grieneisen@jic.ac.uk or sabrina.sabatini@uniroma1.it.

This article contains supporting information online at www.pnas.org/lookup/suppl/doi:10.1073/pnas.1705833114/-/DCSupplemental.

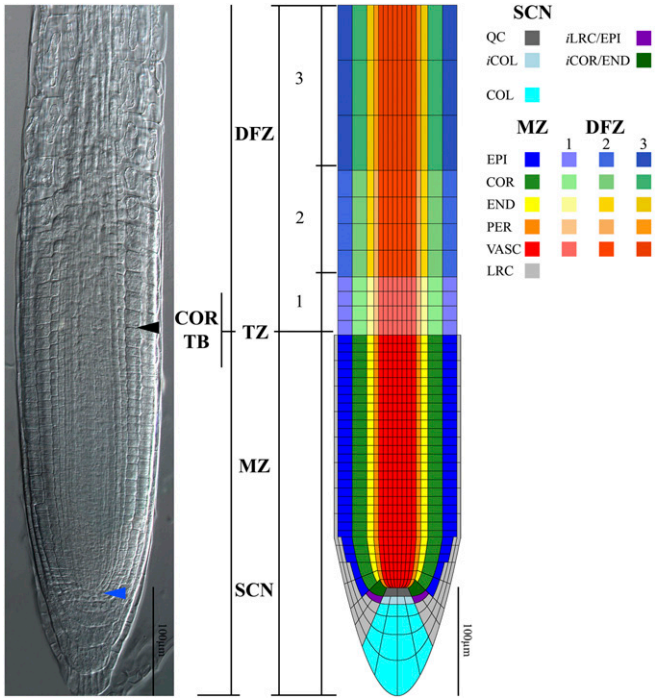

Fig. 1. Root layout. Root zonation at 5 d after germination (dag) in vivo (*Left*) and in silico (*Right*) displaying the stem cell niche (SCN), the meristem zone (MZ), and the differentiation zone (DFZ 1, 2, and 3). In the in silico root layout, the transition zone (TZ) is approximated as a straight boundary, taking the position of the cortex transition boundary (COR TB, blue arrowhead) as reference. Root tissues in the in silico root are color coded. COL, columella; COR, cortex; END, endodermis; EPI, epidermis; *i*COL, columella initial; *i*COR/END, cortex/endodermis initial; *i*LRC/EPI, lateral root cap/epidermis initial; LRC, lateral root cap; PER, pericycle; QC, quiescent center; VASC, vasculature. (Scale bar, 100 μm.)

time scales (order of days) in a logarithmically slowing fashion (9). This, however, is in stark contrast to our in vivo analysis of TZ dynamics in which a shootward shift occurs only within 5 d after germination (dag), followed by an abrupt TZ stabilization (8).

Given that TZ stabilization depends on cytokinin activity, we here extend our previous model introducing the effect of this hormone on auxin transport to understand how this influences graded auxin distribution and thus TZ positioning. In particular, we wish to understand if the patterning dynamics unleashed by the auxin–cytokinin interaction is sufficient to explain TZ positioning, a phenomenon which previous modeling failed to capture.

Results

Cytokinin-Dependent Control of Auxin Polar Transport Is Not Sufficient to Describe the Observed Auxin Graded Distribution. We developed a model in which root-specific features were integrated, using our previous model as a starting point. Auxin distribution in the root was analyzed within a static root tissue, as auxin flows are rapid compared with tissue growth (9, 11). This is in agreement with our experimental setting performed at 5 dag when the root meristem size is set. In our root layout, the TZ is approximated by a single boundary coinciding with the cortex TB (Fig. 1 and *SI Appendix*, Table S1 and *SI Materials and Methods*). To define the root layout, we quantified sizes and shapes of cells of tissues and developmental zones in real roots (Fig. 1 and *SI Appendix*, Table S1 and *SI Materials and Methods*). The resulting in silico root section is connected to a shoot-derived auxin influx into the stele (*SI Appendix*, Table S2 and *SI Materials and Methods*). Reaction terms include basal auxin production and decay in all cells and an auxin source at the SCN (*SI Appendix*, Table S2 and *SI Materials and Methods*). Auxin flows arise from free diffusion within cells and in the apoplast, passive leakage into and out of cells, AUX1-, LAX2-, and LAX3-dependent apolar influx (11), and polar PIN-dependent efflux (*SI Appendix*, Fig. S1 *A–C* and Table S2).

To understand the contribution of cytokinin on auxin distribution, we introduced into the model its repressing effect on PIN1, PIN2, PIN3, and PIN7 activity in the root (4, 12). To quantify this effect, we measured PIN proteins in all tissues and zones of roots expressing *PIN1:GFP*, *PIN2:GFP*, *PIN3:GFP*, and *PIN7:GFP* translational fusions (*SI Appendix*, Table S3 and *SI Materials and Methods*). PIN expression was higher in the MZ than in the DFZ, in agreement with a primary cytokinin effect at the TZ (4) (*SI Appendix*, Fig. S2*A* and Table S3). These measurements were incorporated into the model as tissue- and zone-specific PIN-dependent transport rates (*SI Appendix*, Fig. S2*A*, Table S3, and *SI Materials and Methods*). Auxin reaction–diffusion dynamics were numerically solved to steady state (*SI Appendix*, Table S2 and *SI Materials and Methods*).

With these new settings, the resulting auxin distribution displays a QC-associated auxin maximum as already reported (9, 13) (Fig. 2*A*). In contrast to our previous modeling results, which presented a smoothly declining auxin gradient (9), in this model auxin rose again in the DFZ of the epidermis and of the cortex tissues generating, in these tissues, an auxin dip (defined as the lowest auxin levels within a cell file) (Fig. 2 *A* and *E*). This is in accordance with reported data where auxin distribution in the root is not described by a smoothly declining gradient but auxin forms a maximum in the QC, declines shootwards, and rises again in the DFZ of all root tissues (14, 15). Thus, the introduction of the cytokinin effect into the model contributes to generate a more truthful auxin distribution although only in the external root tissues.

Auxin Graded Distribution Depends on Cytokinin Control of Auxin Polar Transport and of Auxin Degradation. To understand the significance of this auxin dip and to assess to what extent it depends on the cytokinin-dependent changes in PIN expression and localization, we compared our cytokinin-affected model to one in which PIN transport properties were kept uniform over the zones (*SI Appendix*, Fig. S2 *B* and *C*, Table S3 and S4, and *SI Materials and Methods*). We also compared it to a model in which meristematic features, such as cell sizes, were extended to all root zones, only allowing PIN transport properties to vary longitudinally as experimentally observed (*SI Appendix*, Fig. S2*D*, Table S4, and *SI Materials and Methods*). Both resulting auxin profiles show the QC-associated auxin maximum and a graded auxin distribution (*SI Appendix*, Fig. S2 *C* and *D*). However, keeping cytokinin-dependent PIN transport properties uniform over the zones compromised the formation of the dip; in contrast, the dip was unaffected when tissue layout features were maintained as meristematic. These results reveal a strong and specific dependency of the auxin dip formation on cytokinin-dependent PIN activity (Fig. 2*A* and *SI Appendix*, Fig. S2 *C* and *D*). We therefore hypothesized that cytokinin, modifying PIN expression levels, could be instructive in positioning the TZ by creating a dip in the auxin profile. However, in our current cytokinin-dependent PIN model, auxin is rising only in the epidermis and cortex tissues of the DFZ, thus an auxin dip is generated only in these tissues (Fig. 2 *A* and *E*). This suggests that additional cytokinin-dependent mechanism may be involved to determine a rise of auxin in all tissues, thereby extending the dip also to the inner tissues. As we previously demonstrate that ARR1 is necessary and sufficient to mediate cytokinin-dependent control of meristem size and TZ position (4, 8), we performed a genome-wide chromatin immunoprecipitation-based microarray experiment (ChIP chip) from plants carrying an ARR1 translational fusion (*pARR1::ARR1-GFP*) (4). We identified 433 putative ARR1 direct targets, among which, two

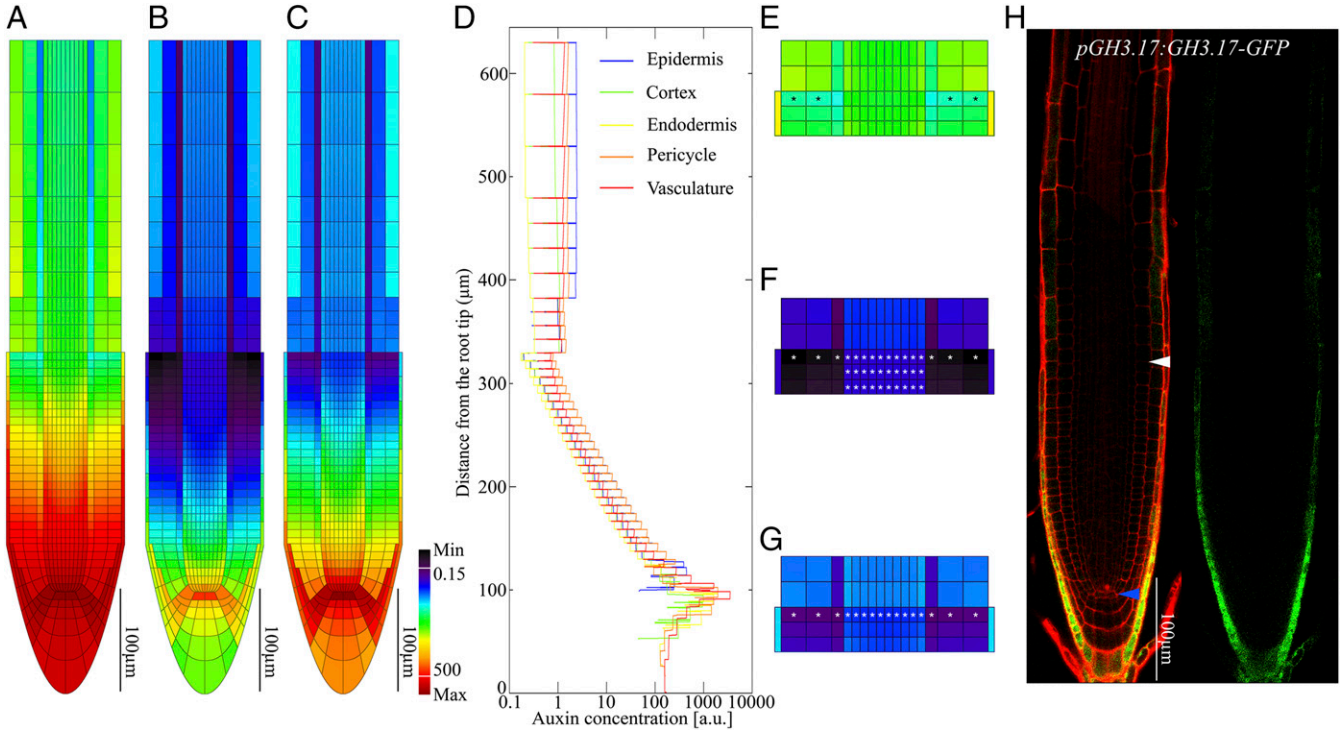

Fig. 2. Local auxin degradation shapes the auxin profile in a well-defined auxin minimum. (*A*–*C*) Predicted steady-state auxin distribution in 5 dag root considering: only the effect of cytokinin regulation on PINs (*A*); cytokinin regulation on PINs together with cytokinin-mediated auxin degradation in all cells (*B*); and cytokinin regulation on PINs together with cytokinin-mediated auxin degradation confined to the GH3.17 expression domain (*C*) (for different setting of parameters used see *SI Appendix*, Table S4). The auxin minimum emerges in the last meristematic cell. Color coding represents auxin concentration levels. (*D*) Longitudinal auxin concentration profiles of simulation in *C* for different tissues, highlighting the formation of the auxin minimum at the TB, in the last meristematic cell of each tissue (*C*, blowup in *G*). Notably the auxin minimum is not formed in simulation in *A* and *B*, as highlighted by the respective blowup in *E* and *F*. Stars in *E*–*G* indicate auxin lowest level within each tissue (dip). Piecewise linear color bar indicates absolute and relative log auxin concentration for all simulations. a.u., arbitrary units. (*H*) Confocal microscopy images of 5 dag root carrying the *pGH3.17:GH3.17-GFP* construct. In *H*, expression of *pGH3.17:GH3.17-GFP* is detected in the same root showing on the *Left* the merged expression of green (GFP) and red [propidium iodide staining (PI)] channels and on the *Right* only the green (GFP) channel. Blue and white arrowheads indicate the QC and the cortex TB, respectively. (Scale bars, 100 μm.)

members of the *GRETCHEN HAGEN 3* (*GH3*) group II family, *GH3.3* and *GH3.17* genes (*SI Appendix*, Table S5 and *SI Materials and Methods*) were found. Members of this gene family mediate auxin conjugation with aspartic and glutamic acid, triggering auxin inactivation (16, 17). As degradation plays an important role in shaping stationary morphogen gradients generated by source–sink mechanisms (18–23), we hypothesized that auxin degradation process impacts on auxin distribution. We therefore introduced in the model the cytokinin-dependent auxin degradation rate (δ_{GH3}) measured in vivo, which was two orders of magnitude higher than the uniform auxin decay rate (δ_{IAA}) used in the previous simulations (*SI Appendix*, Table S2 and *SI Materials and Methods* for parameter derivation and experimental estimates).

We first considered cytokinin-induced auxin degradation acting uniformly over the whole simulated root segment (*SI Appendix*, Table S4). The resulting auxin distribution exhibits an increase of auxin levels in all tissues of the DFZ, with the dip now appearing also in the inner tissues (Fig. 2 *B* and *F*). Thus, auxin degradation is the parameter necessary to ensure a rise of auxin levels in all tissues of the DFZ.

Local Auxin Degradation Generates an Auxin Minimum in the Uppermost Meristematic Cell. To determine if auxin degradation mediated by the *GH3* genes is indeed homogeneously distributed throughout the root, we generated a *GFP* translational fusion of the *GH3.17* gene (*pGH3.17:GH3.17-GFP* plants). We focused on *GH3.17* because we confirmed that *GH3.17* is an ARR1 direct target by ChIP-qPCR analysis (*SI Appendix*, Fig. S3 *A* and *B*), while *GH3.3* expression is unaffected in the *arr1–3* mutant background (*SI Appendix*, Fig. S3*D*). Furthermore, *GH3.17* is induced in an ARR1-overexpressing line and by cytokinin treatment but not by auxin treatment (*SI Appendix*, Fig. S3 *C* and *E–I*). Our analysis of *pGH3.17:GH3.17-GFP* plants revealed that the GH3.17 protein is specifically expressed in the outermost file of columella and lateral root cap (LRC) and in the differentiated epidermal cells (Fig. 2*H*). This expression pattern is consistent with a direct role of the ARR1 protein in controlling *GH3.17* transcriptional activation, given that ARR1 is expressed also in the LRC and differentiated epidermis (*SI Appendix*, Fig. S4*A*). To determine how such GH3.17 specific expression impacts auxin distribution, we confined, in our model, auxin degradation to the observed GH3.17 expression domain (Fig. 2*H* and *SI Appendix*, Fig. S4*B*). Interestingly, the corresponding steady-state profile reveals the auxin dips restricted and aligned specifically to the uppermost meristematic cells of all tissues (Fig. 2 *C*, *D*, and *G* and *SI Appendix*, Fig. S4*C*). This is in contrast to a uniform auxin degradation profile, where the dip does not occur only in the topmost meristematic cells, but a large region of low, constant auxin values in the MZ right below the TZ was observed (Fig. 2 *B* and *F*). We called this well-defined concavity in the auxin profile "auxin minimum." The auxin minimum is defined by the following features: (*i*) it is the lowest auxin level (dip) within the tissue; (*ii*) it occurs only in the uppermost meristematic cell of each tissue thereby aligning in a cell row; and (*iii*) auxin values flanking the dip rise steeply (Fig. 2 *C*, *D*, and *G* and *SI Appendix*, Fig. S4*C*). This auxin minimum is an emergent

property of the entire root system as it is neither a direct result of prepatterned zonation nor occurs at the specific location of auxin degradation. In fact, presence or absence of each of the individual zonation-dependent properties (e.g., cell size, lateral root cap length, and PIN permeability) alone cannot account for the formation or loss of the auxin minimum (*SI Appendix*, Fig. S5 and *SI Materials and Methods*). We, thus, view the root and its spatial complexity as acting synergistically with cytokinin regulation of PINs and auxin degradation to promote the creation of a well-defined auxin minimum.

The Auxin Minimum Can Be Observed in Vivo and Determines the Position of the TZ. The occurrence of the auxin minimum specifically at the location where cells acquire differentiation properties suggests that it may act as a positional signal necessary to trigger the developmental switch from division to differentiation. This is consistent with the view that low auxin levels drive cell differentiation (24–27), and suggests that relative local concentrations can inform developmental decisions.

We first sought to experimentally verify the existence of the auxin minimum in planta and to this end we used the *R2D2* reporter line developed to monitor in vivo auxin levels (28). In line with our in silico observations, the highest value of the n3xVenus/ntdTomato ratio, corresponding to the lowest level of auxin activity, was measured in the topmost meristematic cell of the cortex tissue (Fig. 3*A* and *SI Appendix*, *SI Materials and Methods*). Furthermore, in line with the modeling prediction of a spatial co-occurrence of the minimum over various tissue files, we observed the lowest level of auxin activity in the epidermis and endodermis tissues in the vicinity of the topmost meristematic cortex cells (Fig. 3*A* and *SI Appendix*, *SI Materials and Methods*).

To verify whether the position of this minimum is indeed under the control of cytokinin and to understand if its position determines the position of the TZ, we analyzed its behavior upon cytokinin treatment. Cytokinin causes a rootward shift of the TZ position and a reduction of meristem size (8). Interestingly, upon 12 h of cytokinin treatment the auxin minimum shifts rootwards into the meristem while no changes in TZ position can be observed yet (Fig. 3*B* and *SI Appendix*, *SI Materials and Methods*). Subsequently, upon 20 h of cytokinin treatment the TZ moves rootward, reestablishing itself exactly at the position of the auxin minimum observed at 12 h, thus inducing a shrinkage of the meristem. The auxin minimum coincides now again with the topmost meristematic cells (Fig. 3*C* and *SI Appendix*, *SI Materials and Methods*). Thus, the cytokinin-dependent shift of the auxin minimum induces a transient rearrangement of the tissues, which after 20 h leads to a reestablishment of the TZ to coincide again with the auxin minimum. These data support the existence of the auxin minimum in vivo and suggest that it is a prerequisite for changes in TZ position, corroborating the hypothesis that this auxin minimum functionally correlates with the position of the TZ.

Perturbation of the Auxin Minimum Results in Changes of TZ Position and Alteration of Root Meristem Size. To further investigate the developmental instructiveness of the auxin minimum, we sought to combine in vivo evidence with in silico perturbations. We

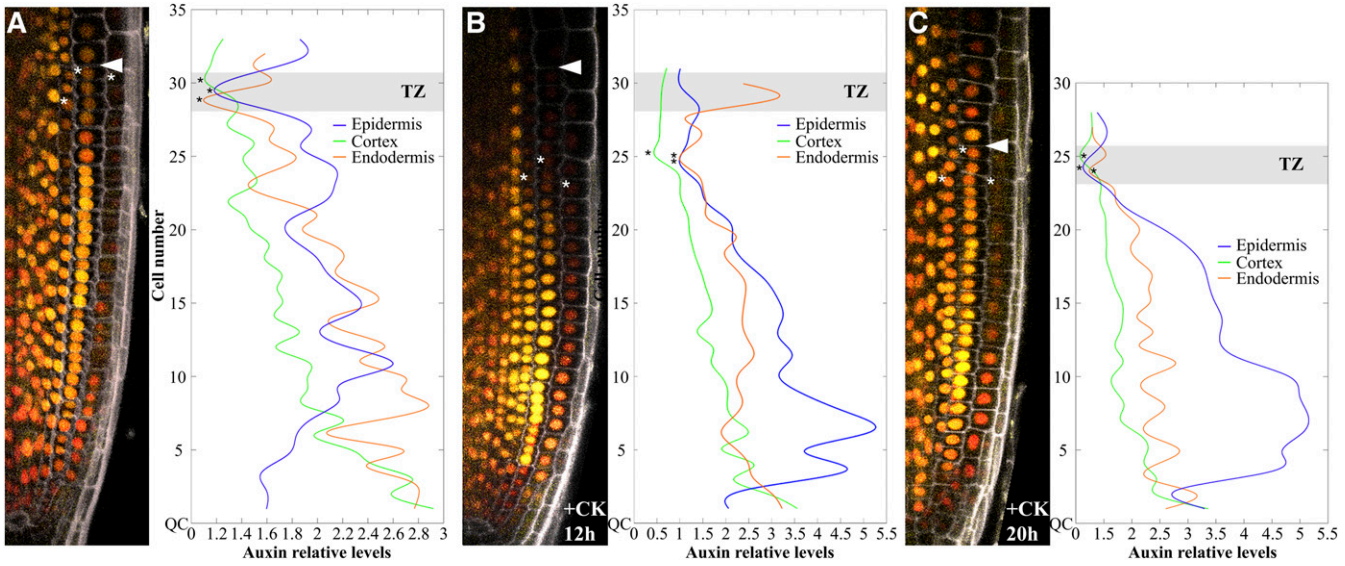

Fig. 3. Auxin minimum quantification in *R2D2* root tip. Maximum projection of confocal z-stack images of untreated (*A*), 12-h cytokinin-treated (+CK 12 h) (*B*) and 20-h cytokinin-treated (+CK 20 h) (*C*) *R2D2* roots (*Left*) with quantification of relative levels of auxin in epidermal, cortex, and endodermal tissues (*Right*). The nuclear signal ratio of n3xVenus/ntdTomato of each cell was normalized to the maximum value of fluorescence intensity (corresponding to a minimum in auxin levels) of the corresponding tissue. Auxin distribution plots (*A*, *Right*; *B*, *Right*; and *C*, *Right*) were derived by reciprocal mean values of the normalized n3xVenus/ntdTomato ratio. Discrete data of measurements in each cell per tissue (blue, epidermis; green, cortex; orange, endodermis) were fitted and plotted as a smooth line (*SI Appendix*, *SI Materials and Methods*). Interestingly a correspondence between the cortex lowest auxin value (cortex dip) (white and black stars) and the last cortex meristematic cell was found (compare *Left* and *Right* in *A*). Epidermis and endodermis dips lay in the proximity of the cortex last meristematic cell defining the auxin minimum position (white and black stars) that coincides with the TZ (gray bar). Upon 12 h of cytokinin treatment (+CK 12 h) (*B*) a rootward shift in the position of the cortex dip (white and black stars) can be observed, although the position of the TZ (gray bar) is unaffected. The epidermis, and endodermis dips also shift rootwards in the proximity of the cortex dip defining the new position of the auxin minimum (white and black stars) (*B*). Upon 20 h of cytokinin treatment (+CK 20 h) (*C*) a shift of the TZ (gray bar) can be observed at the position of the auxin minimum (white and black stars). Moreover, in the 12-h cytokinin-treated roots the auxin minimum for all analyzed tissues lies at the same position as in the 20-h cytokinin-treated roots (compare *B* and *C*). White stars indicate cells where the auxin lowest value (dip) (black stars) was quantified. The region including the dips for each tissue defines the transition zone (TZ) (gray bar in the plot). White arrowhead indicates cortex TB. ANOVA analysis was conducted to determine if differences between the fluorescence detected in the last meristematic cells and the other cells were significant ($P < 0.05$, $n = 22$ for MS and 20-h cytokinin-treated roots; $P < 0.05$, $n = 17$ for 12-h cytokinin-treated roots). Adjusted P values for multiple comparisons were carried out with the Benjamini and Hochberg [false discovery rate (FDR)] method ($P < 0.05$). QC, quiescent center. (Magnification: 40×.)

reasoned that if the auxin minimum is required to position the TZ, its perturbation should result in an altered root meristem phenotype.

Our model predicts that both in the absence of local GH3.17-mediated auxin degradation (Figs. 2*A* and 4*E* and *SI Appendix*, Table S4) and in the case of uniform auxin degradation (Figs. 2*B* and 4*H* and *SI Appendix*, Table S4) the minimum is compromised. In the absence of GH3.17-mediated auxin degradation, the auxin minimum is not reaching low values (Figs. 2*A* and 4*E*), whereas when auxin degradation is imposed in all cells, the auxin minimum presents a very flat auxin profile, with comparable low auxin levels extending over multiple cells within a cell file, thus failing to form the characteristic curvature that constitutes the minimum profile (Figs. 2*B* and 4*H*). As hypothesized, such perturbations affect meristem size: the meristem of the loss-of-function *gh3.17–1* mutant was larger and the root longer than wild type (Fig. 4 *A*, *C*, and *I–K*), while plants ectopically expressing GH3.17 by means of the *UBQ10* promoter (*UBQ10::GH3.17* plants) showed meristems and roots significantly shorter than wild type (Fig. 4 *A*, *F*, and *I–K*). Thus, the experimental data are consistent with the model's predictions showing that local auxin degradation is involved in positioning the TZ and suggest that if the auxin minimum is not established, the position of the TZ is unstable, altering meristem size.

To understand if the altered position of the TZ observed in the *gh3.17–1* mutant and overexpressing line still correlates with an auxin minimum, we simulated these mutants by perturbing the level of auxin degradation accordingly and altering the in silico root layouts according to the observed changes in meristem size. Interestingly, in both simulations the auxin minimum is established at the new TZ position (Fig. 4 *D* and *G* and *SI Appendix*, Table S4 and *SI Materials and Methods*). Thus, cytokinin-dependent auxin degradation induces a rearrangement of auxin levels over the spatial dimensions of the root, reestablishing the auxin minimum at a new location: in the *gh3.17–1* mutant, in which auxin degradation decreases (causing an increase in auxin levels), the position of the auxin minimum shifts shootwards, thus delaying cell differentiation activity, thereby increasing root meristem size. Accordingly, in *UBQ10::GH3.17* roots, where auxin degradation increases (causing a decrease in auxin levels), the auxin minimum shifts rootwards, thus causing a premature initiation of cell differentiation and a shrinkage of the meristem.

In the *gh3.17–1* mutant, our model predicts that local auxin degradation affects the level and distribution of the hormone in the entire root, not only in the GH3.17 domain of expression (Figs. 2*H* and 4 *B*, *D*, and *E*). This is due to the diffusible nature of auxin and the tissue-level reflux loop established by PIN polar transport (9, 23, 29). As a consequence, the *gh3.17–1* mutant presents a changed auxin profile throughout the root and not just within the GH3.17 expression domain. Although mass spectrometry analysis failed to reveal significant changes in free auxin levels in this mutant root tip (probably due to technical limits in detecting small variations in auxin content in specific regions), it revealed much lower levels of IAA-glutamate (IAGlu) than in the wild type (Fig. 4 *L* and *M*). Moreover, the analysis of DR5 and DII-VENUS reveals significant changes in their expression level (Fig. 4*N* and *SI Appendix*, Fig. S6), in accordance with the model prediction in which the QC auxin maximum is maintained and changes in auxin levels are mainly observed in the meristem (compare Fig. 4*B* with Fig. 4*D*).

Given that the position of the auxin minimum also depends on cytokinin-mediated regulation of auxin transport via SHY2, we investigated whether also in this mutant the reported changes in meristem size (4) can be explained by a repositioning of the auxin minimum. Simulations where SHY2-dependent PIN repression is removed while maintaining GH3.17-dependent local auxin degradation, capturing the *shy2* mutant effects, displayed a loss of the auxin minimum (*SI Appendix*, Fig. S7*A*). The minimum was however fully reestablished in simulations that took the enlarged meristem observed in the *shy2* mutant into account (*SI Appendix*, Fig. S7*B* and Table S4).

These data support the notion that the presence of an auxin minimum is necessary to position the TZ and that changes in its position result in changes in root meristem size.

Cytokinin-Dependent Local Auxin Degradation and Transport Are both Necessary for the Positioning of the Auxin Minimum. The model predicts that the auxin minimum position depends on auxin transport, affected via SHY2, and auxin degradation, modified through GH3.17. To verify this notion in vivo, we analyzed the *R2D2* reporter line in the *gh3.17–1* and *shy2-31* mutants.

As predicted, the auxin minimum in these mutants coincides with the position of the TZ (Fig. 5*C* and *SI Appendix*, Fig. S8*A*). Furthermore, upon cytokinin treatments, whereas in wild-type plants the auxin minimum and the TZ shifted rootwards and the root meristem shrank (Figs. 3 and 5 *A* and *B*), neither in the *gh3.17–1* nor in the *shy2-31* mutant were the positions of the auxin minimum and TZ affected, and the size of the meristem was unaltered (Fig. 5 *C* and *D* and *SI Appendix*, Fig. S8 *A* and *B*). Thus, both the SHY2 and the GH3.17 proteins are necessary to position the auxin minimum and the TZ and involved in controlling meristem size in response to cytokinin. Analysis of the double mutant, *shy2-31;gh3.17–1*, revealed an enlarged root meristem and longer root than either parent, suggesting that they have an additive effect on meristem size (Fig. 6).

Cytokinin Effects on Auxin Minimum Explain How Cytokinin Regulates Root Meristem Size. Finally, we explored the effect of modifications in cytokinin level on the auxin minimum and thereby meristem size (4, 8). We simulated the effect of cytokinin depletion by removing local auxin degradation and concomitantly increasing PIN permeability (*SI Appendix*, Table S4 and *SI Materials and Methods*). Under these conditions, the auxin minimum in the topmost meristematic cells was impaired (Fig. 7 *A* and *B*), suggesting that these cells, without the correct signal, would delay entering the differentiation program and continue to proliferate causing an increase of the meristem, consistent with the behavior of cytokinin-deficient plants (4, 8) and the enlarged meristem observed in the double, *shy2-31;gh3.17–1* mutant. Indeed, increasing the number of meristematic cells in the root layout based on in vivo observations reestablished the minimum at the TZ (Fig. 7 *A* and *C*). Likewise, simulations capturing the effects of cytokinin treatment, where local auxin degradation was increased and PIN permeability decreased (*SI Appendix*, Table S4 and *SI Materials and Methods*), failed to generate the auxin minimum (Fig. 7 *A* and *D*). Instead, these simulations showed a rootward-shifted gradient with an extended flat region of low auxin concentrations in the MZ, suggesting premature cell differentiation (Fig. 7 *A* and *D*). An auxin minimum localized at the TZ was reestablished, with its characteristic high concavity, solely by decreasing the number of cell rows in the MZ (Fig. 7 *A* and *E*) accounting for the meristem shrinkage observed in cytokinin-treated plants (4, 8).

Discussion

Understanding how boundaries are maintained during organ growth is a fundamental question in developmental biology. In *Arabidopsis*, the size of the root meristem and root growth are determined by the position of the TZ, a developmental boundary that separates dividing cells from cells that will undergo differentiation (8). By controlling polar auxin distribution, cytokinin maintains the position of this boundary during root growth and determines root meristem size (4). Here, by means of a systems biology approach based on the mutual feedback of model predictions and in vivo observations, we show that cytokinin

maintains the position of the TZ controlling not only polar auxin transport but also auxin degradation. In particular, besides regulating auxin polar transport in the inner root tissues by repressing PIN expression via SHY2 (4), we show here that the

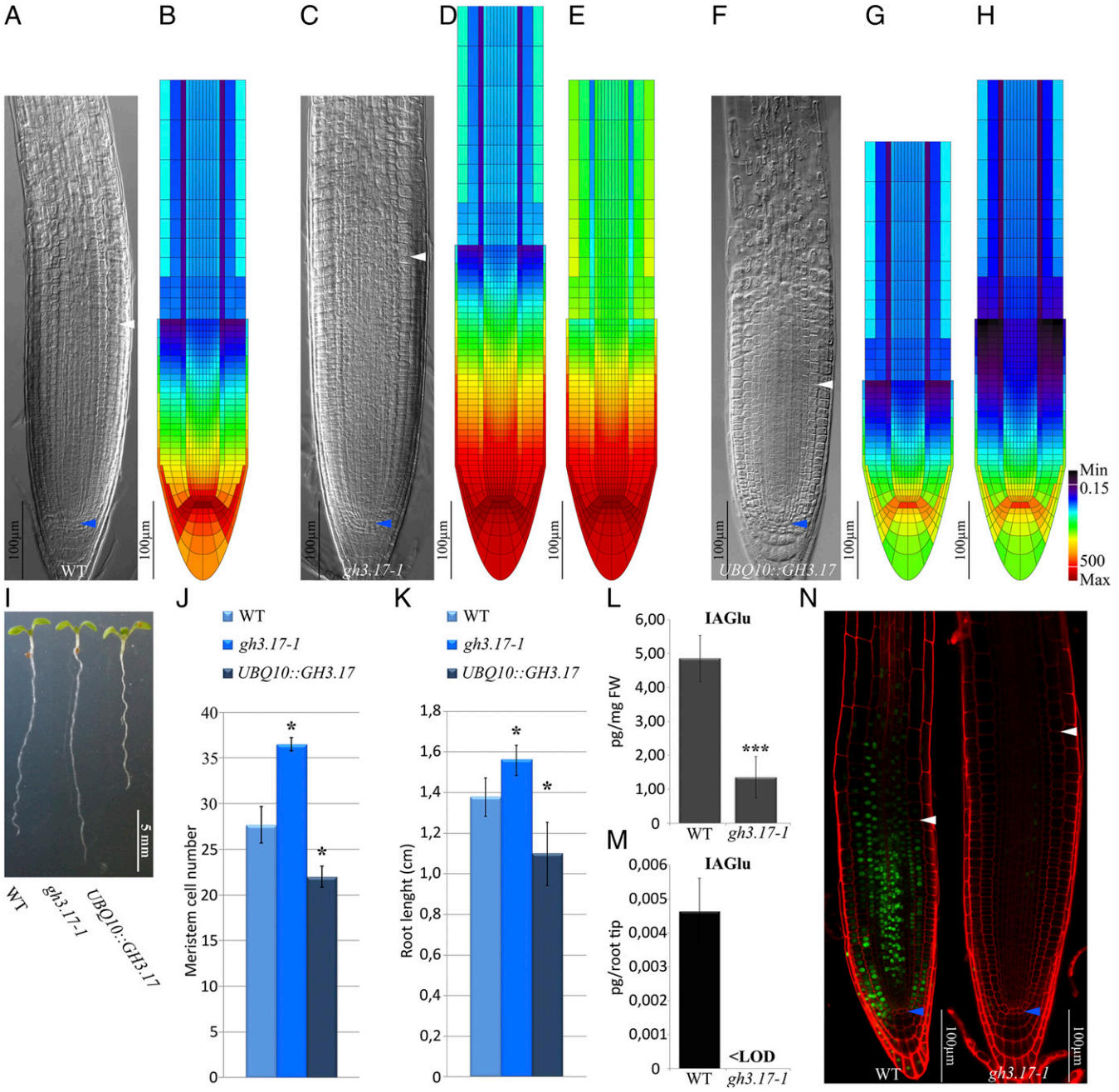

Fig. 4. The cytokinin-dependent auxin minimum correlates with the position of the transition zone. (*A*) WT root at 5 dag and its predicted steady-state auxin pattern in *B*. (*C*) *gh3.17–1* root at 5 dag. (*D* and *E*) Predicted steady-state auxin pattern in the *gh3.17–1* mutant (*D*) compared with the simulation obtained considering only the effect of cytokinin on PINs and excluding the GH3.17-dependent tissue-specific auxin degradation (*E*). Note that the auxin minimum is absent in *E* and is reestablished in *D* where the number of MZ cells in the root layout was increased according to the *gh3.17–1* root phenotype (*E*). (*F*) Root of *UBQ10::GH3.17* overexpressing line at 5 dag. (*G* and *H*) Auxin heat map of *UBQ10::GH3.17* overexpressing root (*G*) compared with simulation where GH3.17-dependent auxin degradation is imposed in all cells (*H*). Note that the auxin minimum is absent in *H* since the low auxin values do not subsequently rise again (i.e., the curvature is low) the characteristic high curvature is reestablished in *G* by decreasing the number of MZ cells in the root layout, according to the *UBQ10::GH3.17* root phenotype (*F*). (*I*) Root phenotype of the *gh3.17–1* mutant and the *UBQ10::GH3.17* overexpressing line. (*J* and *K*) Changes in meristem size (*J*) and root length (*K*) of the *gh3.17–1* mutant and the *UBQ10::GH3.17* overexpressing line. (*L* and *M*) Mass spectrometry quantification of IAA-glutamate (IAGlu) in WT and *gh3.17–1* whole roots and 1-mm root tips. Limit of detection for IAGlu = 0.5 fmol. (*N*) Analysis of *DII-VENUS* expression in the *gh3.17–1* mutant highlighting higher auxin activity as predicted in *D*. A total of 20 plants for two biological replicates were analyzed. (Scale bars, 100 µm.) Color coding represents auxin concentration levels. Piecewise linear color bar indicates absolute and relative log auxin concentration for all simulations. Blue and white arrowheads indicate the QC and the cortex TB, respectively. *Statistically significant difference in the *gh3.17–1* and *UBQ10::GH3.17* versus WT ($n = 30$ each sample, three biological replicates; Student *t* test, $P < 0.05$. ***Statistically significant difference in the *gh3.17–1* versus WT lines in an ANOVA analysis (*t* test; $P < 0.001$). Error bars indicate SD.

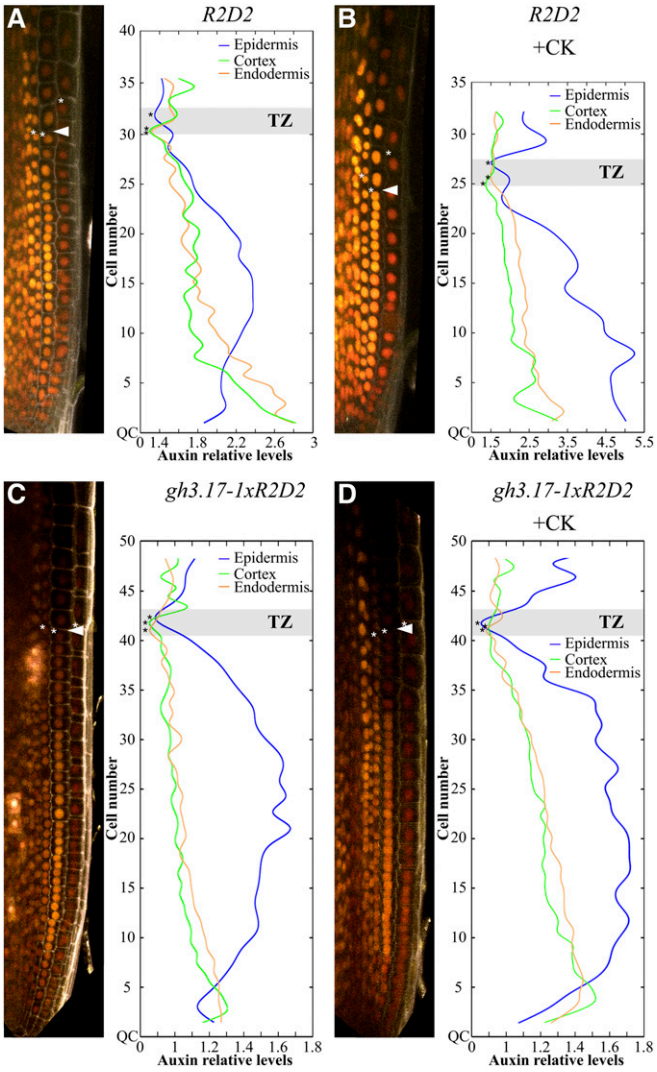

Fig. 5. GH3.17 is necessary for the positioning of the auxin minimum. Maximum projection of confocal z-stack images of *R2D2* and *gh3.17–1xR2D2* (*Left*) with quantification of relative levels of auxin in epidermal, cortex, and endodermal tissues (*Right*). The roots represent untreated *R2D2* plant (*A*), *gh3.17–1xR2D2* plant (*C*), cytokinin-treated (+CK) *R2D2* plant (*B*), and *gh3.17–1xR2D2* plant (*D*). Auxin distribution plots (*Right*) were derived by discrete data of measurements in each cell per tissue (blue, epidermis; green, cortex; and orange, endodermis) (*SI Appendix, SI Materials and Methods*). A correspondence between the cortex lowest auxin value (cortex dip, white and black stars) and the last cortex meristematic cell was found (compare *Left* and *Right*). Epidermis and endodermis dips lay in the proximity of the cortex last meristematic cell defining the auxin minimum position (white and black stars) that coincides with the TZ (gray bar). Upon cytokinin treatment, a rootward shift in the position of the cortex, epidermis, and endodermis dip (white and black stars) can be observed in *R2D2* roots (*B*), but not in *gh3-17–1xR2D2* (*D*). White stars indicate cells where the auxin lowest value (dip) (black stars) was quantified. White arrowhead indicates cortex TB. ANOVA analysis was conducted to determine if differences between the fluorescence detected in the last meristematic cells and the other cells were significant ($P < 0.05$, $n = 33$ for MS and 20-h cytokinin-treated *R2D2* roots; $P < 0.05$, $n = 39$ for MS and 20-h cytokinin-treated *gh3-17–1xR2D2* roots). Adjusted *P* values for multiple comparisons were carried out with the Benjamini and Hochberg (FDR) method ($P < 0.05$). QC, quiescent center. (Magnification: 40×.)

cytokinin-dependent transcription factor ARR1 directly controls auxin degradation in the external tissues by inducing the expression of the gene *GH3.17*. The combined control of transport and degradation determines changes in relative auxin levels that generate a minimum of this hormone specifically localized in the topmost meristematic cells of each tissue, where the transition from cell division to cell differentiation occurs (Fig. 8). The model reveals that the expression domain of GH3.17, where the highest rate of auxin degradation occurs, does not colocalize with the minimum itself. The uncoupling between the degradation domain and the position of the minimum, as well as the dependency of the positioning of the minimum on the level of degradation, results from the underlying auxin reflux loop (23). The auxin reflux loop redistributes auxin to form characteristic gradient in the root apex and results from the entanglement that exists between auxin production, degradation, and transport. The resultant auxin gradient has an auxin maximum located at the QC (9), while an auxin minimum lays at the last meristematic cell.

Our results reveal that the auxin minimum is always functionally correlated with the position of the TZ: changes in TZ position and meristem size are preceded by movement of the auxin minimum (Fig. 3), which determines the new TZ position. Furthermore, while it suffices to affect auxin polar transport or degradation to change the position of the auxin minimum, and thus of the TZ, both processes are necessary to stabilize the

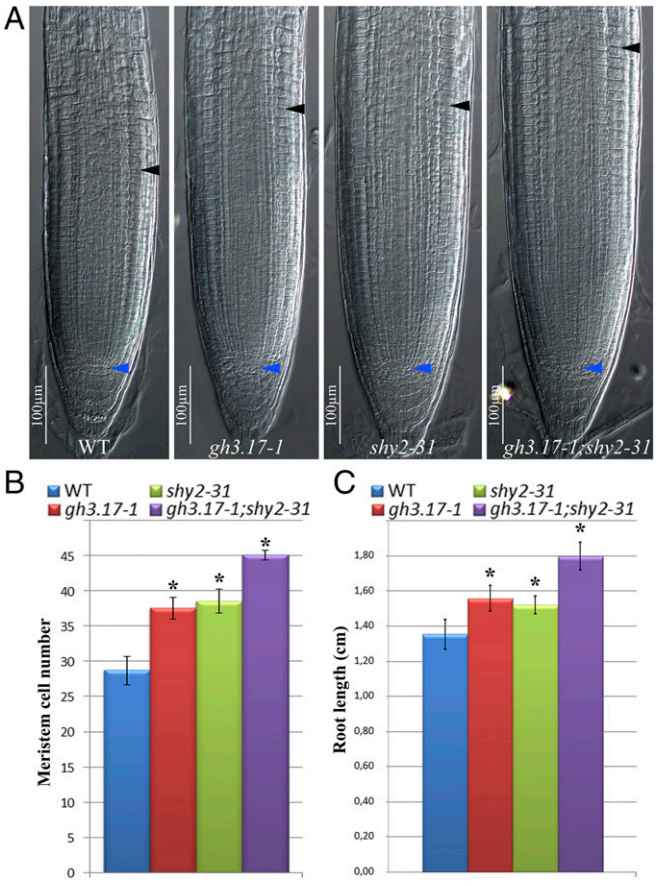

Fig. 6. GH3.17 and SHY2 have additive effects on TZ positioning. (*A*) Root meristem of WT, *gh3.17–1*, *shy2-31*, and *shy2-31;gh3.17–1* double mutant. (*B*) Analysis of root meristem size of WT, *gh3.17–1*, *shy2-31*, and *shy2-31; gh3.17–1* double mutant. (*C*) Analysis of root length of WT, *gh3.17–1*, *shy2-31*, and *shy2-31;gh3.17–1* double mutant. Note that the *shy2-31;gh3.17–1* double mutant displays both a longer meristem and root than the parental, suggesting that these genes have an additive effect on TZ positioning. Blue arrowheads point to the QC and black arrowheads indicate the cortex TB. Error bars represent SD of results from three biological replicates. *Significant difference from the WT (Student *t* test, $P < 0.05$). (Scale bars, 100 μm.)

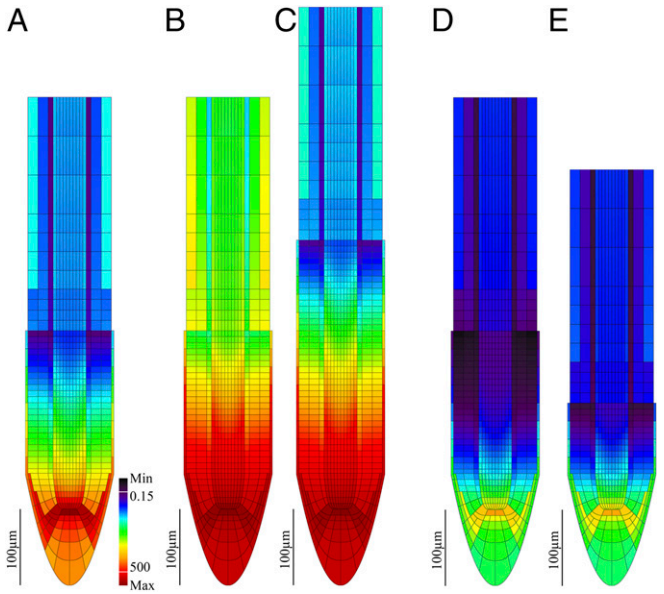

Fig. 7. Cytokinin-dependent regulation of auxin degradation and transport is essential to shape the auxin gradient. (*A*) Steady-state auxin heat map of wild-type root. (*B*) Predicted steady-state auxin pattern in simulation mimicking the effect of cytokinin depletion that results in increased PIN expression and decreased GH3.17 expression. Auxin minimum formation is affected. (*C*) The auxin minimum reestablishes only by increasing the number of MZ cells in the root layout. (*D*) Predicted steady-state auxin pattern in simulation mimicking the effect of exogenous cytokinin application that results in decreased PIN expression and increased GH3.17 expression. Such changes in PIN and GH3.17 expression prevent the formation of the auxin minimum. (*E*) The auxin minimum is reestablished by decreasing the number of MZ cells in the root layout. (Scale bars, 100 μm.) Color coding represents auxin concentration levels. Piecewise linear color bar indicates absolute and relative log auxin concentration for all simulations.

position of the auxin minimum and maintain meristem size. We therefore propose that this auxin minimum acts as a positional signal that triggers the developmental switch from cell division to cell differentiation.

The peculiar feature of this auxin minimum consists in having the lowest auxin level (dip) within each tissue aligned in a cell row. This alignment of dips ensures the coordinated activity of the cells where the dip occurs, so that these cells will switch together to the differentiation program thus preserving the root structure and zonation.

It should be pointed out that the consistent correspondence between cytokinin-driven auxin minimum formation and root zonation reveals that auxin patterning guides the localization and stabilization of the TZ in a self-organizing manner where cytokinin may operate along with other inputs (27) (*SI Appendix*, Fig. S5). Recently, it has been demonstrated that programmed cell death of the lateral root cap establishes the pattern for lateral root formation by releasing pulses of auxin to the neighboring tissues (30). Future challenge will be to understand how the position of the auxin minimum correlates with the programmed cell death of the LRC and how these two inputs are coordinated to control the dynamic of root growth and the entire root system organization.

The identification of the auxin minimum at the TZ, together with the previous identification of a distal auxin maximum (31), provides compelling evidence of the instructive role of auxin in positioning multiple developmental outputs, in strong analogy with morphogenetic gradients in animals. At the auxin minimum, the auxin level of cells belonging to different tissues is different (Fig. 2 *C*, *D*, and *G* and *SI Appendix*, Fig. S4*C*). This suggests that an absolute auxin threshold is not needed to trigger cell differentiation. Thus, our analysis of TZ specification in the *Arabidopsis* root suggests that it may be insightful to reconsider morphogenetic gradient theory in terms of context-dependent profile features, such as minima with an inherent curvature, instead of absolute thresholds only.

Materials and Methods

Plant Material and Growth Conditions. The *Arabidopsis thaliana* ecotypes *Columbia-0* (*Col-0*) and *Landsberg erecta* (*Ler*) were used. *gh3.17–1* mutant (16) is in the *Col-0* background and the *shy2-31* mutant (4) is in the *Ler* background. *gh3.17–1* mutant was obtained from the Nottingham *Arabidopsis* Stock Centre collection (Salk_050597). Homozygous mutants from the Salk T-DNA were identified by PCR as described (http://signal.salk.edu/). *shy2-31* mutant was genotyped by cleaved amplified polymorphic sequences; the amplicon (*SI Appendix*, Table S6) was digested with Hpy188III.

pARR1::ARR1:GUS, *DR5::GFP*, *DII-VENUS*, and *R2D2* transgenic plants have been described previously (8, 13, 15, 28).

For growth conditions, *Arabidopsis* seeds were surface sterilized, and seedlings were grown on one-half strength Murashige and Skoog (MS) medium containing 0.8% agar at 22 °C in long-day conditions (16-h-light/8-h-dark cycle) as previously described (32).

Arabidopsis locus IDs from this article are as follows: *ACTIN2* (AT3G18780), *UBQ10* (AT4G05320), *ARR1* (AT3G16857), *GH3.3* (AT2G23170), *GH3.17* (AT1G28130), and *IAA3/SHY2* (AT1G04240).

Code Availability. All simulations were performed using in-house developed computer code written in C. A remote repository has been used for the code (Git repository) as well as the scripts that generated all simulation outputs

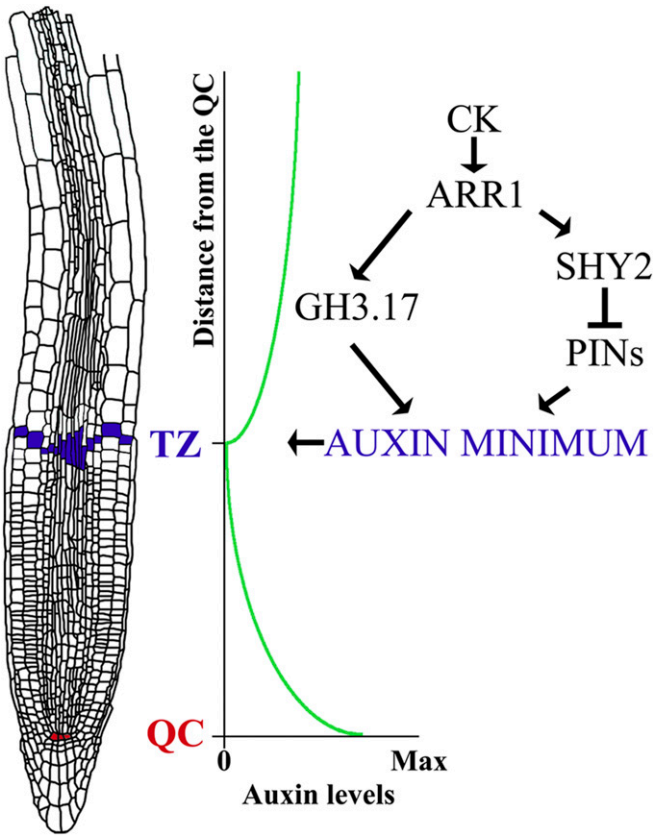

Fig. 8. Proposed model. Cytokinin (CK), through ARR1, controls both auxin catabolism (via positive regulation of GH3.17) and polar transport (via positive regulation of SHY2). As a result, auxin profile is shaped, generating a developmental instructive auxin minimum. The auxin minimum acts as a signal that positions the TZ and drives meristematic cells toward differentiation.

(graphs and images) presented in the main text and figures and discussed in *SI Appendix, SI Materials and Methods*. Access to the repository is available on Bitbucket (https://bitbucket.org/mareelab/transitionzone).

Computer Model. A description of the computer model of auxin transport in the *Arabidopsis* root is contained in the *SI Appendix, SI Materials and Methods*.

Accession Code. The Gene Expression Omnibus Database accession no. is GSE70595.

More detailed information regarding the experimental and computational procedures used in this study is provided in *SI Appendix, SI Materials and Methods*.

ACKNOWLEDGMENTS. We thank Ben Scheres for reading the manuscript; Leonardo Giustini and Raffaele Dello Ioio for technical support; Dolf Weijers for providing *R2D2* seeds; Valerio Licursi for help on statistical analysis; and GrassRoots Biotechnology, Inc. for providing the *pDONORP4P1-pUBQ10* vector, pub. no. WO/2012/006426. This work was supported by European Research Council Grant 260368 (to S.S., R.D.M., M.D.R., and E.P.), Istituto Pasteur-Fondazione Cenci Bolognetti (S.S. and P.C.), Progetti di Rilevante Interesse Nazionale of Ministero dell'Istruzione, dell'Università e della Ricerca (P.C., L.D.P., and M.D.R.), UK Biological and Biotechnology Research Council Grant BB/J004553/1 to the John Innes Centre (to V.A.G. and A.F.M.M.), and European Commission 7th Framework Program, Project 601062, Swarm-Organ (to V.A.G.). R.D.M. and M.D.R. were also supported by a short-term European Molecular Biology Organization Fellowship (ASTF 260-2011/Award and ASTF 209-2013/Award).

1. Wolpert L (1989) Positional information revisited. *Development* 107:3–12.
2. Rogers KW, Schier AF (2011) Morphogen gradients: From generation to interpretation. *Annu Rev Cell Dev Biol* 27:377–407.
3. Dahmann C, Oates AC, Brand M (2011) Boundary formation and maintenance in tissue development. *Nat Rev Genet* 12:43–55.
4. Dello Ioio R, et al. (2008) A genetic framework for the control of cell division and differentiation in the root meristem. *Science* 322:1380–1384.
5. De Rybel B, et al. (2014) Plant development. Integration of growth and patterning during vascular tissue formation in Arabidopsis. *Science* 345:1255215.
6. Chaiwanon J, Wang ZY (2015) Spatiotemporal brassinosteroid signaling and antagonism with auxin pattern stem cell dynamics in Arabidopsis roots. *Curr Biol* 25:1031–1042.
7. Benfey PN, Scheres B (2000) Root development. *Curr Biol* 10:R813–R815.
8. Dello Ioio R, et al. (2007) Cytokinins determine *Arabidopsis* root-meristem size by controlling cell differentiation. *Curr Biol* 17:678–682.
9. Grieneisen VA, Xu J, Marée AFM, Hogeweg P, Scheres B (2007) Auxin transport is sufficient to generate a maximum and gradient guiding root growth. *Nature* 449:1008–1013.
10. Petersson SV, et al. (2009) An auxin gradient and maximum in the *Arabidopsis* root apex shown by high-resolution cell-specific analysis of IAA distribution and synthesis. *Plant Cell* 21:1659–1668.
11. Band LR, et al. (2014) Systems analysis of auxin transport in the *Arabidopsis* root apex. *Plant Cell* 26:862–875.
12. Ruzicka K, et al. (2009) Cytokinin regulates root meristem activity via modulation of the polar auxin transport. *Proc Natl Acad Sci USA* 106:4284–4289.
13. Ulmasov T, Murfett J, Hagen G, Guilfoyle TJ (1997) Aux/IAA proteins repress expression of reporter genes containing natural and highly active synthetic auxin response elements. *Plant Cell* 9:1963–1971.
14. Santuari L, et al. (2011) Positional information by differential endocytosis splits auxin response to drive Arabidopsis root meristem growth. *Curr Biol* 21:1918–1923.
15. Brunoud G, et al. (2012) A novel sensor to map auxin response and distribution at high spatio-temporal resolution. *Nature* 482:103–106.
16. Staswick PE, et al. (2005) Characterization of an *Arabidopsis* enzyme family that conjugates amino acids to indole-3-acetic acid. *Plant Cell* 17:616–627.
17. Ljung K (2013) Auxin metabolism and homeostasis during plant development. *Development* 140:943–950.
18. Lander AD (2007) Morpheus unbound: Reimagining the morphogen gradient. *Cell* 128:245–256.
19. Kicheva A, et al. (2007) Kinetics of morphogen gradient formation. *Science* 315:521–525.
20. Kolomeisky AB (2011) Formation of a morphogen gradient: Acceleration by degradation. *J Phys Chem Lett* 2:1502–1505.
21. Wartlick O, Kicheva A, González-Gaitán M (2009) Morphogen gradient formation. *Cold Spring Harb Perspect Biol* 1:a001255.
22. Wartlick O, et al. (2011) Dynamics of Dpp signaling and proliferation control. *Science* 331:1154–1159.
23. Grieneisen VA, Scheres B, Hogeweg P, M Marée AF (2012) Morphogengineering roots: Comparing mechanisms of morphogen gradient formation. *BMC Syst Biol* 6:37.
24. Laskowski M, et al. (2008) Root system architecture from coupling cell shape to auxin transport. *PLoS Biol* 6:e307.
25. Sorefan K, et al. (2009) A regulated auxin minimum is required for seed dispersal in Arabidopsis. *Nature* 459:583–586.
26. Perrot-Rechenmann C (2010) Cellular responses to auxin: Division versus expansion. *Cold Spring Harb Perspect Biol* 2:a001446.
27. Mähönen AP, et al. (2014) PLETHORA gradient formation mechanism separates auxin responses. *Nature* 515:125–129.
28. Liao CY, et al. (2015) Reporters for sensitive and quantitative measurement of auxin response. *Nat Methods* 12:207–210, 2 p following 210.
29. Blilou I, et al. (2005) The PIN auxin efflux facilitator network controls growth and patterning in *Arabidopsis* roots. *Nature* 433:39–44.
30. Xuan W, et al. (2016) Cyclic programmed cell death stimulates hormone signaling and root development in *Arabidopsis*. *Science* 351:384–387.
31. Sabatini S, et al. (1999) An auxin-dependent distal organizer of pattern and polarity in the *Arabidopsis* root. *Cell* 99:463–472.
32. Perilli S, Sabatini S (2010) Analysis of root meristem size development. *Methods Mol Biol* 655:177–187.